



Critical behavior of Fredenhagen-Marcu string order parameters at topological phase transitions with emergent higher-form symmetries



Wen-Tao Xu^{1,2} , Frank Pollmann^{1,2} & Michael Knap^{1,2} 

A nonlocal string order parameter detecting topological order and deconfinement has been proposed by Fredenhagen and Marcu (FM). However, due to the lack of exact internal symmetries for lattice models and the nonlinear dependence of the FM string order parameter on ground states, it is a priori not guaranteed that it is a genuine order parameter for topological phase transitions. In this work, we find that the FM string order parameter exhibits universal scaling behavior near critical points of charge condensation transitions, by directly evaluating the FM string order parameter in the infinite string-length limit using infinite Projected Entangled Pair States (iPEPS) for the toric code in a magnetic field. Our results thus demonstrate that the FM string order parameter represents a quantitatively well-behaved order parameter. We find that only in the presence of an *emergent* 1-form symmetry the corresponding FM string order parameter can faithfully detect topological transitions.

Since the discovery of the fractional quantum Hall effect^{1,2}, topological phases of matter have been intensively explored. Exactly solvable models have been constructed^{3–5}, and a mathematical framework for classifying topological phases of matter has been developed^{6,7}. Recently, various topologically ordered states have been experimentally investigated with quantum computers and simulators as well^{8–10}. Unlike conventional phases of matter, topological phases cannot be characterized by simple local order parameters. Instead non-local string order parameters are required, for example, as proposed by Fredenhagen and Marcu (FM) in the context of the \mathbb{Z}_2 gauge-Higgs model^{11–14}. Recently, this FM string order parameter has also been used to detect \mathbb{Z}_2 topological order in a quantum dimer model realized by the Rydberg quantum simulator^{9,15}. The construction of the FM order parameter is based on the following idea. In the presence of an exact Wilson loop symmetry, which is an exact 1-form symmetry^{16–21}, the charge condensation transition can be detected using a string order parameter carrying charges at the two ends. However, in the absence of the exact 1-form Wilson loop symmetry, the expectation value of the string order parameter decays exponentially to zero with the string length. Therefore, it cannot be used to detect phase transitions anymore. This problem is circumvented by the FM string order parameter in which the expectation value of the string operator is divided by the square root of the expectation value of a Wilson loop operator of doubled length, such that the exponential decay caused by explicitly violating the exact 1-form Wilson loop symmetry is canceled, see Fig. 1a.

In contrast to the usual definition of the order parameters for spontaneous symmetry-breaking phases and symmetry-protected topological phases, the FM order parameter is not defined based on the exact symmetry of the model, and the FM string order parameter is a non-linear function of the ground states. Therefore, it is not guaranteed that the FM string order parameter is quantitatively well-behaved, i.e., one cannot ensure that the FM string order parameter is smooth in a gapped phase and continuous when crossing a second-order phase transition. Even more so, it is unclear whether the FM string order parameter exhibits critical behavior, as usual order parameters do, in the vicinity of a quantum critical point.

In this work, we study properties of the FM string order parameter of the toric code model in a field and elucidate the role of emergent higher-form symmetries. We evaluate the FM string order parameter associated with charge excitations in the limit of an infinitely long string using transfer matrices of infinite Projected Entangled Pair States (iPEPS). Technically, we approximate ground states of the model using variational iPEPS optimization^{22,23}, in which energy gradients are calculated by automatic differentiation²⁴. We find that near the topological transition between the toric code and the Higgs region, Fig. 1b, the FM string order parameter exhibits a critical exponent of the $(2 + 1)$ D Ising* universality class²⁵. In the presence of the electric-magnetic (EM) duality symmetry, the phase transition has been previously studied with a local order parameter^{26–28}. We show that the FM string order parameter exhibits critical scaling in the vicinity of

¹Technical University of Munich, TUM School of Natural Sciences, Physics Department, 85748 Garching, Germany. ²Munich Center for Quantum Science and Technology (MCQST), Schellingstr. 4, 80799 München, Germany. ✉e-mail: wen-tao.xu@tum.de

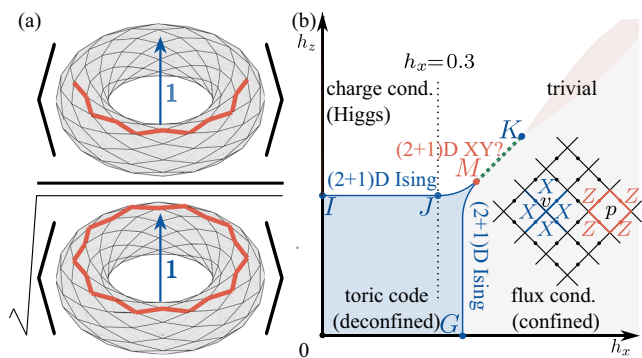


Fig. 1 | FM string order parameter and phase diagram. **a** Schematic of the FM string order parameter associated with charge excitations, where black lines indicate the underlying lattice on a torus, red lines are a string and a loop of Z operators, respectively, and 1 is the trivial anyon flux penetrating through the torus. **b** Phase diagram of the (2+1)D toric code model in a field, including a toric code phase (blue region), a duality symmetry breaking phase (green dotted line along MK) and a trivial phase (white+red+gray regions). The trivial phase is separated into three regions by emergent 1-form symmetries: the charge condensation region (white) with the emergent Wilson loop symmetry and the flux condensation region (gray) with the emergent 't Hooft loop symmetry, as well as a region without any emergent 1-form symmetry (red). Boundaries of regions in the trivial phase are shown schematically. Inset: definition of the vertex and the plaquette operators on a square lattice.

this phase transition but with a new critical exponent, which is different from that of the local order parameter. The universality of this multi-critical point has been recently under debate^{26–29} because although the numerical results from the scaling of local operators are consistent with the multi-critical point belonging to the XY^* universality class, the semionic statistics between charge and flux is not included in the XY^* field theory in an obvious way. We find the critical exponent from the FM string order parameter to be compatible with the (2 + 1)D XY^* universality class as well. However, due to the comparatively large numerical uncertainty this does not rule out other field theoretic descriptions of the multi-critical point. In general, our results show that despite being a nonlinear function of the ground state, the FM string order parameter exhibits universal scaling behavior near critical points, suggesting that it is a quantitatively well-behaved order parameter for topological phase transitions accompanied by charge condensation.

We emphasize that the FM string order parameter associated with charge excitations can only be used to reliably detect topological phase transitions when the ground states possess an emergent 1-form Wilson loop symmetry in the infrared (blue and white shaded regions in Fig. 1b). Thus, some prior knowledge of the underlying higher-form symmetries are needed when applying the FM string order parameter to a model with an unknown phase diagram. For instance, in the flux condensation region (gray region in 1b) in which there is no emergent 1-form Wilson loop symmetry, the FM order parameter can be a discontinuous function (i.e., it jumps from zero to a finite value) of ground states even in the absence of phase transitions. Moreover, in the absence of an emergent 1-form symmetry we find the FM order parameter to be numerically unstable for variational iPEPS, see Supplemental Materials³⁰ (similar observations were found in Monte Carlo simulations^{12,31}). In particular, a dual FM string order parameter associated with magnetic flux is required to detect the topological flux condensation transition where an emergent 1-form 't Hooft loop symmetry exists [blue and gray shaded region in Fig. 1b].

Results

Toric code model and the FM string order parameter

We consider the toric code model on a square lattice in a field:

$$H_{TC}(h_x, h_z) = - \sum_v A_v - \sum_p B_p - h_x \sum_e X_e - h_z \sum_e Z_e, \quad (1)$$

where $A_v = \prod_{e \in v} X_e$ and $B_p = \prod_{e \in p} Z_e$ are the vertex and plaquette operators, as shown in the inset of Fig. 1b, and X_e and Z_e are Pauli matrices defined on the edges e of the lattice. The phase diagram of the model in Fig. 1b consists of a toric code phase at weak fields and a trivial phase at strong fields^{32–34}.

Recent work has introduced higher-form symmetries to describe topological order^{16–21}. For certain choices of the magnetic fields, the toric code model in Eq. (1) has exact 1-form symmetries that commute with the Hamiltonian: (i) for $h_x = 0$, the 1-form Wilson loop symmetry commutes with $H_{TC}(0, h_z)$, $[\prod_{e \in L} Z_e, H_{TC}(0, h_z)] = 0$, where L is a closed loop on the primal lattice and (ii) for $h_z = 0$ the 1-form 't Hooft loop symmetry commutes with $H_{TC}(h_x, 0)$, $[\prod_{e \in \tilde{L}} X_e, H_{TC}(h_x, 0)] = 0$, where \tilde{L} is a closed loop on the dual lattice. (On a torus, the 1-form symmetries include both contractible and non-contractible loop operators, while on a sphere the 1-form symmetries only consist of contractible loop operators.) Crucially, even when the exact symmetries are explicitly broken, higher-form symmetries can still be emergent at low energies, capturing the robustness of topological order. Concretely, both of the 1-form symmetries are emergent in the toric code phase, see Fig. 1b. In this formalism, topological order can be interpreted as a spontaneous breaking of such emergent symmetries, drawing analogies to conventional symmetry breaking phases^{19–21,35,36}. Furthermore, the trivial phase can be separated into several regions by emergent 1-form symmetries^{26,35}. The charge condensation region (white area in Fig. 1b), also known as the Higgs region, only has the emergent 1-form Wilson loop symmetry. The flux condensation region (gray area in Fig. 1b), also known as the confined region, only has the emergent 1-form 't Hooft loop symmetry. The red area in Fig. 1b does not possess any of the two emergent 1-form symmetries.

As the toric code model in Eq. (1) has the exact 1-form Wilson loop symmetry at $h_x = 0$, a string operator $\prod_{e \in L_{1/2}} Z_e$ creates a pair of charges at its two ends, where $L_{1/2}$ is an open string along the primal lattice. Thus, a string order parameter \tilde{O}_Z can be constructed to detect charge condensation³⁷:

$$\tilde{O}_Z = \lim_{|L_{1/2}| \rightarrow \infty} \sqrt{|\tilde{C}_Z(|L_{1/2}|)|}, \quad \tilde{C}_Z(|L_{1/2}|) = \langle \Psi | \prod_{e \in L_{1/2}} Z_e | \Psi \rangle, \quad (2)$$

where $|\Psi\rangle$ is a normalized ground state of the toric code model, $|L_{1/2}|$ is the distance between two ends of $L_{1/2}$. The bulk of the string order parameter \tilde{O}_Z commutes with the overlapping local Hamiltonian terms but not its ends. In the toric code phase, the string order operator thus creates two anyonic charge excitations that are orthogonal to the ground state, leading to a vanishing string order parameter in the infinite string limit, $\tilde{O}_Z = 0$. By contrast, in the Higgs phase, the string order parameter can be nonzero because the h_z field induces charge fluctuations such that charges condense in the Higgs phase. The string order parameter can also be interpreted as the “disorder parameter” of the exact 1-form Wilson loop symmetry. In the deconfined topological phase, where the ground states spontaneously break the exact 1-form Wilson loop symmetry, the string order parameter vanishes. Conversely, the Higgs regime is disordered under the exact 1-form Wilson loop symmetry and the string order parameter is nonzero. An alternative way of interpreting this string operator is by mapping $H_{TC}(0, h_z)$ to the (2 + 1)D transverse field Ising model^{38,39}. This transforms \tilde{O}_Z and \tilde{C}_Z to the Ising order parameter and its correlation function, respectively. From that also follows directly that the critical point I [see Fig. 1b] at $h_z = h_{zc}^{(I)} = 0.328474(3)$ ⁴⁰ belongs to the (2 + 1)D Ising* universality class, where the “*” indicates that in the effective Ginzburg-Landau-Wilson theory the order parameter field ϕ can only be created in pairs and ϕ and $-\phi$ are physically indistinguishable²⁵. Near the critical point I : $\tilde{O}_Z \sim (h_z - h_{zc}^{(I)})^\beta$ and $\xi \sim (h_z - h_{zc}^{(I)})^{-\nu}$, where $\beta = 0.326418(2)$ is the critical exponent of the order parameter⁴¹, ξ is the correlation length defined via $|\tilde{C}_Z(|L_{1/2}|) - \tilde{O}_Z^2| \sim e^{-|L_{1/2}|/\xi}$, and $\nu = 0.629970(4)$ is the critical exponents of the correlation length⁴¹.

When $h_x \neq 0$, the Wilson loop operator $\prod_{e \in L} Z_e$ is no longer an exact 1-form symmetry of the toric code model and the bulk of the string $\prod_{e \in L_{1/2}} Z_e$ cannot deform freely. Therefore $\tilde{C}_Z(|L_{1/2}|)$ vanishes on either side of the topological phase transition exponentially with the length of the

Table 1 | Z string and Z loop operators

	$h_x = 0^{37}$		$h_x = 0^{38}$		$h_x \& h_z \neq 0^{12}$
	deconf.	Higgs	deconf.	confined	
$\langle \prod_{e \in L} Z_e \rangle$	1	1	$e^{-\alpha_z L }$	$e^{-\alpha'_z S_L}$	$e^{-\alpha_z L }$
$\langle \prod_{e \in L_{1/2}} Z_e \rangle$	$e^{-\alpha' L_{1/2} }$	$O(1)$	0	0	$e^{-\alpha_z L_{1/2} }$

The behavior of Z loop (string) operator, defined as $\langle \prod_{e \in L} Z_e \rangle$ ($\langle \prod_{e \in L_{1/2}} Z_e \rangle$), are known from the references. When $h_z = 0$, the ground states have the exact 1-form 't Hooft loop symmetry which anti-commutes Z-string operator, therefore $\langle \prod_{e \in L_{1/2}} Z_e \rangle = 0$. $|L|$ ($|L_{1/2}|$) denotes the length of the loop (string) and S_L is the size of the area surround by the loop L . α_z and α'_z are coefficients depending on details of models.

string $|L_{1/2}|$. However, when h_x is small, the toric code model has an emergent 1-form Wilson loop symmetry^{17,26,35}. In the limit of large h_x , the 1-form Wilson loop symmetry cannot emerge, which we indicate by the gray and red areas in Fig. 1b. In the presence of an emergent 1-form Wilson loop symmetry, one can in principle conceive to construct a dressed string operator with an extended width^{2,43}. This is however a challenging task in practice. This problem can be circumvented, by dividing out the “bulk” contribution of the string order parameter, as proposed by Fredenhagen and Marcu, leading to the FM string order parameter^{11,12}:

$$O_Z = \lim_{r \rightarrow \infty} \sqrt{|C_Z(r)|}, \quad C_Z(r) = \frac{\langle \Psi | \prod_{e \in L_{1/2}} Z_e | \Psi \rangle}{\sqrt{\langle \Psi | \prod_{e \in L} Z_e | \Psi \rangle}}, \quad (3)$$

where $r = |L_{1/2}|$ is the length of the string $L_{1/2}$. Notice that $|L_{1/2}|$ should be understood as the length of $L_{1/2}$ instead of the distance between its two ends because the bulk of the Z-string cannot be deformed freely when $h_x \neq 0$. In addition, for the \mathbb{Z}_2 gauge Higgs model, we should replace the string operator $\prod_{e \in L_{1/2}} Z_e$ with $Z_v \left(\prod_{e \in L_{1/2}} Z_e \right) Z_{v'}$, where v and v' are two vertices at the ends of the string $L_{1/2}$. L is a loop whose length is twice the length of the string $L_{1/2}$, see Fig. 1a. Compared to Eq. (2), the FM string order parameter in Eq. (3) contains a square root of the expectation value of the Wilson loop operator in the denominator. When $h_x \neq 0$ the bare Wilson loop operator is no longer a symmetry and its expectation values decays in the presence of an emergent 1-form symmetry of charge excitations with a perimeter law (except in the flux condensation phase with exact 1-form 't Hooft loop symmetry ($h_z = 0$), where the expectation value of the bare Wilson loop operator decays with an area law): $\langle \Psi | \prod_{e \in L} Z_e | \Psi \rangle \sim \exp(-\alpha_z |L|)$, where α_z is the perimeter law coefficient and $|L|$ is the length of the loop L . The denominator in the FM string order parameter compensates the perimeter law decay of the numerator, such that only the contribution from the endpoints of the string $L_{1/2}$ is taken into account, where charges are created. We also separately summarize the behaviors of the numerator and denominator of the FM string order parameter in Table 1, from which we immediately see that the FM string order parameter is always 0 when $h_z = 0$ and it cannot detect the phase transition between the deconfined phase and the confined phase. In addition, we emphasize that the FM string order parameter is a nonlinear function of the ground state. Therefore, one needs to carefully analyze whether it can serve as a bona fide order parameter for topological phase transitions.

We now use iPEPS algorithms to directly evaluate the FM string order parameter in the limit of infinitely long strings on a torus, see Methods. When L is a non-contractible loop on the torus, which is convenient for tensor network methods, care has to be taken when evaluating the denominator in Eq. (3), as it could vanish for certain linear combinations of the degenerate ground states. Nonetheless, we are able to show that contractible and non-contractible loops are equivalent when the ground state is a minimally entangled state⁴⁴ with a trivial anyon flux penetrating through the torus; Fig. 1a. Therefore, we use this choice for the ground state in the

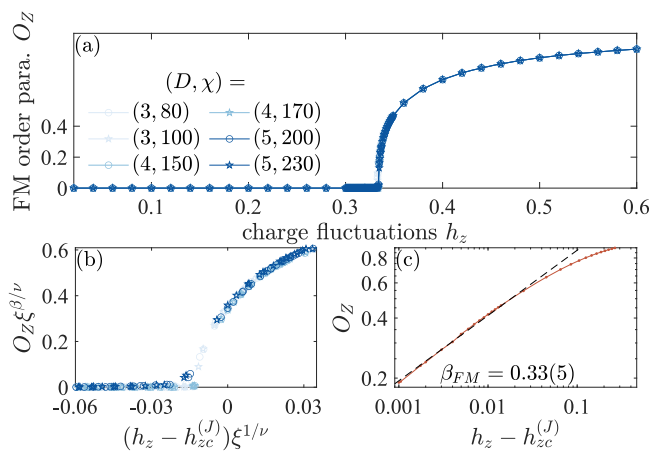


Fig. 2 | FM string order parameter of the variational iPEPS along $h_x = 0.3$. **a** The FM string order parameter from iPEPS with various bond dimensions (D, χ), see legend, is continuous across the topological phase transition. **b** Data collapse of the FM string order parameter with $\nu = 0.629970(4)$ and $\beta = 0.326418(2)$. **c** Double-log plot used for extracting the critical exponent β_{FM} from the scaling of O_Z in the vicinity of the critical point, where we used $h_{zc}^{(J)} = 0.335(1)$. Data is obtained by linearly extrapolating O_Z in the inverse iPEPS bond dimension $1/D$.

numerical evaluation of the FM order parameter; technical details are discussed in the Methods section.

FM string order parameter of the variational wave function

We will now analyze the general properties of the FM string order parameter across a topological phase transition with charge condensation. In particular, we want to analyze whether the FM string order parameter is continuous upon crossing a second-order phase transition, and if so, we will analyze its scaling behavior. To this end, we first consider a cut through the phase diagram at $h_x = 0.3$, that crosses the transition line IM in Fig. 1b at a point J . The criticality of the topological transition along the line IM is expected to be described by the $(2 + 1)D$ Ising* universality class. There are two important parameters that systematically control the error of the approximation when numerically evaluating the FM string order parameter: the bond dimension D of the iPEPS itself and the bond dimension χ of the environment of the iPEPS; the larger bond dimensions provide better approximations. Therefore, we evaluate FM string string order parameter numerically along $h_x = 0.3$ from iPEPS with various bond dimensions, see Fig. 2a. From this we find the critical point J on the $h_x = 0.3$ line is at $h_z = h_{zc}^{(J)} = 0.335(1)$, consistency with $h_{zc}^{(J)} = 0.333(1)$ from previous quantum Monte Carlo simulation⁴⁰. In the toric code phase, the FM string order parameter vanishes while it is finite in the Higgs phase.

Crucially, the FM string order parameter is continuous across a second order phase transition, such that we can extract the critical exponent β_{FM} defined via $O_Z \sim (h_z - h_{zc}^{(J)})^{\beta_{FM}}$, Fig. 2c, where we obtain O_Z by performing linear extrapolation in $1/D$ and ignore the small χ dependence. The extracted critical exponents $\beta_{FM} = 0.33(5)$ is consistent with the exponent $\beta = 0.326418(2)$ of the $(2 + 1)D$ Ising* universality class⁴¹, see Table 2 for a summary of the exponents. We furthermore collapse the data from different bond dimensions, as shown in Fig. 2b, based on the theory of finite entanglement scaling⁴⁵⁻⁴⁷. The data for $D > 2$ indeed collapses on a single curve near criticality. These results show that the FM string order parameter exhibits the correct critical behavior controlled by the $(2 + 1)D$ Ising* universality class near the critical point J .

Previous order parameters for topological phase transitions were defined on the virtual legs of the iPEPS⁴⁸⁻⁵², because there exist the virtual symmetries in terms of matrix product operators⁵³⁻⁵⁵. However, without the iPEPS representation, these virtual order parameters cannot be obtained, i.e., they are not physical. This should be contrasted with the FM string order parameter that is defined on the physical level and thus also does not depend on the iPEPS gauge.

Next, we consider the FM string order parameter of the variational wave function along the self-dual line $h_x = h_z$, where the toric code model in Eq. (1) has a global electric-magnetic duality symmetry, which exchanges the primal lattice and the dual lattice, as well as X and Z . There is a gapped electric-magnetic duality symmetry breaking phase MK along the self-dual line^{26,32,33}. The transition between the toric code phase and the duality symmetry breaking phase is a multi-critical point M shown in Fig. 1b. From our iPEPS simulation we find that M is located at $h_x = h_z = h_{zc}^{(M)} = 0.3397(2)$, which is again close to $0.340(2)$ from the quantum Monte Carlo simulations³² and to $0.3406(4)$ obtained from the higher-order perturbation expansion³³. The phase transition crossing the multi-critical point M can be characterized by a local symmetry-breaking order parameter $|\langle X - Z \rangle|$, which is the difference between expectation values of X_e and Z_e on a single edge e , as shown in Fig. 3a, from which we extract a critical exponent $\beta_{\text{local}} = 0.83(5)$ defined via $|\langle X - Z \rangle| \sim (h_z - h_{zc}^{(M)})^{\beta_{\text{local}}}$, see Fig. 3c. Our result is consistent with recent Monte Carlo simulation²⁶. We also evaluate the FM string order parameter along the self-dual line crossing the multi-critical point M ; Fig. 3d. For the FM string order parameter, we extract the critical exponent $\beta_{\text{FM}} = 0.34(4)$ defined via $O_Z \sim (h_z - h_{zc}^{(M)})^{\beta_{\text{FM}}}$, Fig. 3f, which is quite different from the critical exponent of the local symmetry-breaking order parameter $\beta_{\text{local}} = 0.83(5)$.

How can we understand the distinct critical exponents β_{local} and β_{FM} ? Since the phase boundary IM belongs to the Ising* universality class and the FM string order parameter exhibits an Ising critical exponent, we can

Table 2 | Critical exponents of the Ising* field theory in (2+1)D and (2+0)D

Exponent	(2 + 1)D	(2 + 0)D
Δ_ϕ	0.518 1489 (10) ⁴¹	1/8 ⁷⁸
Δ_{ϕ^2}	1.412 625 (10) ⁴¹	1 ⁷⁸
$\nu = (D - \Delta_{\phi^2})^{-1}$	0.629 970 (4)	1
$\beta = \Delta_\phi \nu$	0.326 418 (2)	1/8
β_{FM} (this work)	0.33 (5)	0.117 (5)

From the scaling dimensions Δ_ϕ and Δ_{ϕ^2} of the fields ϕ and ϕ^2 , respectively, one obtains the correlation length exponent ν and critical exponent of the order parameter β , where D is the spacetime dimension. Critical exponent of the FM string order parameter β_{FM} obtained from iPEPS in this work. The critical exponents β and β_{FM} are consistent.

assume that the FM string order parameter O_Z corresponds to a field ϕ_z of an effective Ginzburg-Landau-Wilson theory describing the Ising* transition. When two Ising* transition lines IM and GM in Fig. 1b meet at the multi-critical point M , one could conceive that the effective field theory of the multi-critical point M is the XY^* model with a Lagrangian $\mathcal{L} = (\partial\phi)^2/2 + m^2\phi^2/2 + g\phi^4/(4!)$ ^{26,27}, up to some irrelevant terms, which possesses $O(2)$ symmetry. Here, $\phi = (\phi_x, \phi_z)$ is a two-component vector field. We summarize the scaling dimensions of the order parameter fields and relevant critical exponents in Table 3. We find that β_{FM} is consistent with β_ϕ and β_{local} with β_- of the XY^* field theory. This can be understood by identifying ϕ_z with the FM string order parameter O_Z , and $\phi_x^2 - \phi_z^2$ with $X - Z$ ²⁶⁻²⁸. We can separately check consistency with the XY^* field theory by performing data collapse of the FM string order parameter and the local order parameter using the critical exponents of the field theory; Fig. 3b and e, where we find a reasonable collapse for iPEPS dimension $D > 3$.

Some comments are in order. First, the two degenerate ground states in the duality symmetry-breaking phase correspond to the predominant condensation of charges (fluxes) satisfying $\langle X - Z \rangle < 0$ ($\langle X - Z \rangle > 0$).

Table 3 | Critical exponents of the XY^* field theory in (2+1)D and (2+0)D

Exponent	(2 + 1)D	(2 + 0)D
Δ_ϕ	0.519088 (22) ⁷⁹	1/8 ⁸⁰
Δ_+	1.51136 (22) ⁷⁹	1 ⁸⁰
Δ_-	1.23629 (11) ⁷⁹	1/2 ⁸¹
$\nu_+ = (D - \Delta_+)^{-1}$	0.67175 (1)	1
$\beta_\phi = \Delta_\phi \nu_+$	0.34870 (7)	1/8
$\beta_- = \Delta_- \nu_+$	0.83048 (2)	1/2
β_{FM} (this work)	0.34 (4)	-
β_{local} (this work)	0.83 (5)	-

Scaling dimensions Δ_ϕ , Δ_+ , and Δ_- of the fields ϕ_z , $\phi^2 = \phi_x^2 + \phi_z^2$, $\phi_x^2 - \phi_z^2$, respectively. From these scaling dimensions, one obtains the critical exponent ν_+ of the correlation length, β_ϕ of the single component of the order parameter ϕ_x , and β_- of the additional order parameter $\phi_x^2 - \phi_z^2$. D is the spacetime dimension. The critical exponent of the FM string order parameter β_{FM} and the local order parameter β_{local} obtained from iPEPS in this work are consistent with β_ϕ and β_- in (2 + 1)D, respectively. In (2 + 0)D, since there is a gapless BKT phase along the self-dual line in Fig. 4a, we can not define β_{FM} and β_{local} .

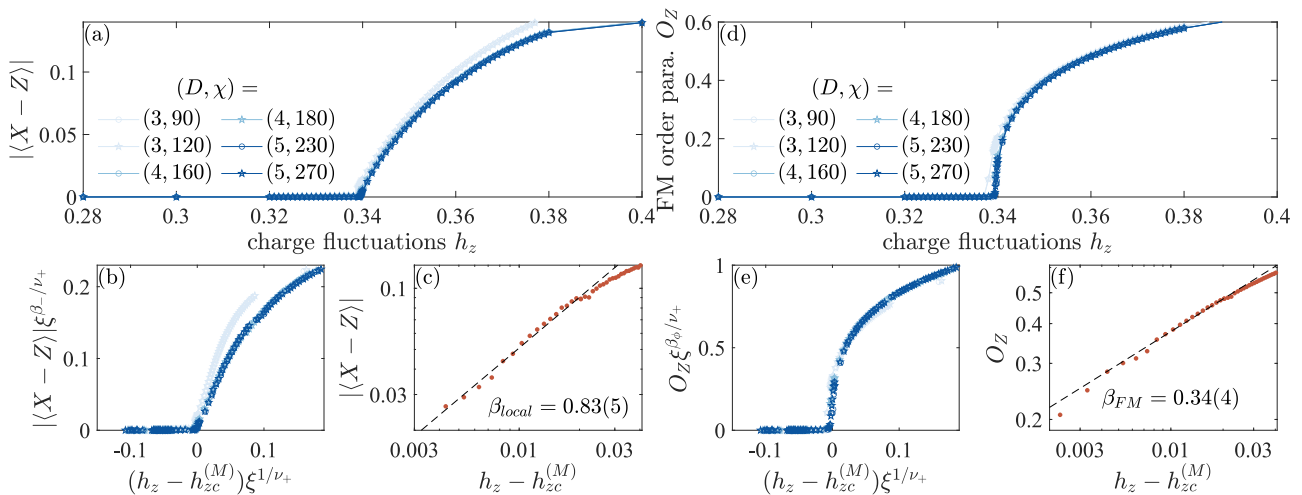


Fig. 3 | Local duality symmetry-breaking and FM string order parameters of the variational iPEPS along the self-dual line $h_x = h_z$. **a** Local order parameter $|\langle X - Z \rangle|$ from iPEPS with various bond dimensions (D, χ) , see legend. **b** Data collapse of the local order parameter with $\nu_+ = 0.67175(1)$ and $\beta_- = 0.83048(2)$. **c** Critical exponent β_{local} , where $|\langle X - Z \rangle|$ is obtained by linear extrapolation in $1/D$ and

$h_{zc}^{(M)} = 0.3397(2)$. **d** FM string order parameter from iPEPS with various bond dimensions, see legend. **e** Data collapse of the FM string order parameter with $\beta_\phi = 0.34870(7)$. **f** Critical exponent β_{FM} , where O_Z is again obtained by linear extrapolation in $1/D$.

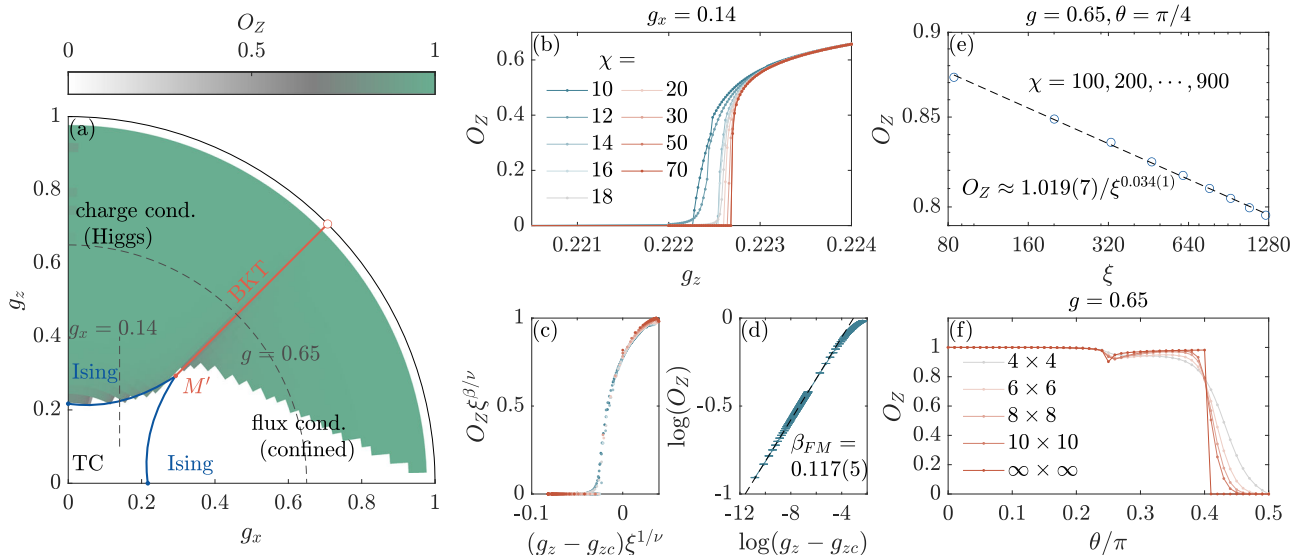


Fig. 4 | FM string order parameter for the deformed toric code wave function. **a** Phase diagram of the deformed toric code state of Eq. 4. We also plot a color-map of the FM order parameter O_Z in the phase diagram. **b** The FM string order parameter along $g_x = 0.14$ [vertical dashed line in **a**], calculated using iMPS with various bond dimensions χ . **c** Data collapse of the FM string order parameter with $g_{zc} = 0.2227(3)$, $\beta = 1/8$ and $\nu = 1$. **d** Critical exponent β_{FM} of the FM string order parameter, obtained by extrapolating O_Z for different χ . **e** Double-log plot of the FM string order

parameter O_Z as a function of the correlation length ξ of the boundary MPS at the point $(g, \theta) = (0.65, \pi/4)$ in the BKT phase. O_Z vanishes in the limit of infinite bond dimension $\chi \rightarrow \infty$. **f** Finite and infinite length FM string order parameters along $g_x^2 + g_z^2 = 0.65^2$ [dashed quarter circle in **a** parametrized with $\theta = \arctan(g_x/g_z)$] from the iMPS with $\chi = 20$. The legend shows the size of the area surrounded by the loop operator.

Because our FM string order parameter is defined with a Z string, it detects the charge condensation, and thus, we should use the charge condensation-dominated state to evaluate the FM string order parameter. In contrast, the dual FM string order parameter associated with the flux excitations is not well-behaved when applied to the same ground state; see Supplemental materials³⁰. Second, ref. 26 argues that the multi-critical point M may not belong to the XY^* universality class because the mutual semionic statistics between charges and fluxes is not included in the XY^* field theory in an obvious way. Although our numerical data is consistent with the XY^* field theory, we cannot rule out other field theoretic descriptions of the transition due to the comparatively large uncertainties in the critical exponents.

FM string order parameter for the deformed toric code state

Instead of variationally solving the ground state Hamiltonian in Eq. (1), one can analytically construct a deformed toric code state, which shares similar physics with the toric code Hamiltonian in Eq. (1). The advantage of the deformed toric code state is that the wavefunction is exact, so many analytical results can be derived. The disadvantage is that the dimensionality of the universality class of the quantum critical points is fine-tuned and reduced by 1 compared to that of the generic quantum critical points^{56,57}. The deformed toric code state is defined as⁵⁸⁻⁶⁰:

$$|\psi(g_x, g_z)\rangle = \prod_e (1 + g_x X_e + g_z Z_e) |TC\rangle, \quad (4)$$

where $|TC\rangle$ is a ground state of the fixed point toric code Hamiltonian, and g_x and g_z are tuning parameters satisfying $g_x^2 + g_z^2 \leq 1$. The phase diagram of the deformed toric code state is similar to that of the toric code Hamiltonian in Eq. (1), as shown in Fig. 4a. Besides the toric code phase, there are two trivial phases with either charge or flux condensation, and they are separated by a Berezinskii-Kosterlitz-Thouless (BKT) transition line. The phase transition lines from the toric code phase to the trivial phase belong to the (2+0)D Ising* universality class because of the dimensionality reduction at the fine-tuned critical points of the wave function. Because the deformed toric code state is mapped to the partition function of the 2D classical Ashkin-Teller model⁶⁰, the multi-critical point $M' = (1 - 1/\sqrt{2}, 1 -$

$1/\sqrt{2})$ at the self-dual line $g_x = g_z$ is described by the free boson conformal field theory (CFT) compactified on orbifolds with a radius $R = 2\sqrt{2}$, which describes the critical point of the 2D XY^* theory⁶¹. Thus, we can say the multicritical point M' of the deformed toric code state belongs to the (2+0) D XY^* universality class.

Akin to the variational case, we first calculate the FM string order parameter along a line $g_x = 0.14$ crossing the toric code phase and the Higgs phase by contracting the $D = 2$ exact iPEPS of the deformed toric code state, using the boundary infinite matrix product states (iMPS) with various bond dimensions χ , see Fig. 4b. We extract the critical exponent β_{FM} of the FM string order parameter according to $O_Z \sim (g_z - g_{zc})^{\beta_{FM}}$, for which we numerically determine the critical point $g_{zc} = 0.2227(3)$ and extrapolate O_Z using different iMPS bond dimensions χ . The extracted $\beta_{FM} = 0.117(5)$ is close to the $\beta = 1/8 = 0.125$ from the 2D Ising* universality class, see Fig. 4d and Table 2. We perform the data collapse to the FM string order parameter in Fig. 4c. These results indicate that the FM string order parameter is a well-behaved order parameter also for the deformed wavefunction. In contrast to the variational case, along the self-dual line the phase transition from the toric code phase to the BKT phase along the self-dual line is not a charge condensation transition, and the FM string order parameter is zero in both the toric code phase and the BKT phase, see Fig. 4e. Therefore, the FM string order parameter cannot be directly used to detect the BKT transition.

The FM string order parameter evaluation of the deformed toric code is numerically stable, since the wave function can be exactly expressed in terms of an iPEPS without the need of variational optimization. We evaluate the FM string order parameter in the entire phase diagram of the deformed toric code state, as shown in Fig. 4a as a color plot, which surprisingly exhibits a sharp transition in the flux condensation phase even in the absence of a quantum phase transition. To emphasize this behavior, we show the FM string order parameter along a path $g_x^2 + g_z^2 = 0.65^2$ in Fig. 4f. It is discontinuous at a certain angle $\theta = \arctan(g_x/g_z) \approx 0.4\pi$ even in the absence of a bulk phase transition. In order to exclude the possibility that there are some artifacts of our method that cause the discontinuity, we also evaluate the FM string order parameter with finite string length $r = \lfloor L_{1/2} \rfloor$ in Fig. 4f. As the string length increases, the results from the thermodynamic limit are obtained, which indeed implies that the FM string order parameter becomes discontinuous for

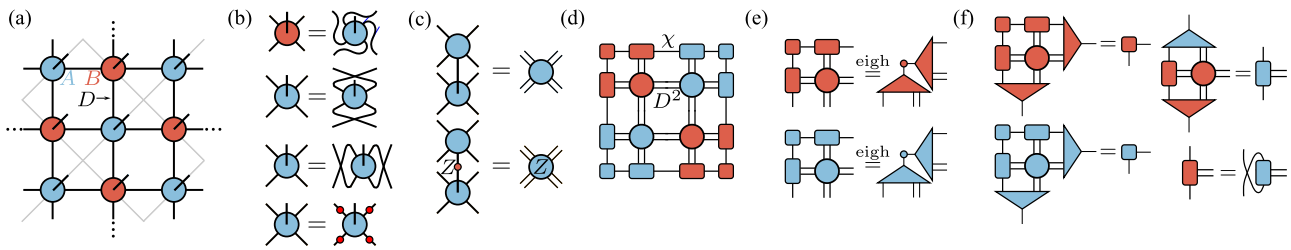


Fig. 5 | iPEPS ansatz and the CTMRG. **a** The iPEPS ansatz for the ground state of the toric code model with a bond dimension D . **b** The iPEPS tensors A and B are related by rotation. The iPEPS tensor A is invariant under two reflections, and we can also impose the virtual \mathbb{Z}_2 symmetry when necessary, where the red dots are matrices Z_D . **c** A double tensor and another double tensor sandwiching a Z matrix.

d The environment of the iPEPS is approximated by the corner tensors (squares) and the edge tensors (rectangles). **e** The hermitian eigenvalue decomposition (eigh) of the top-left corner of the tensor networks in **d**, the isometries can be obtained from eigenvectors corresponding to the χ largest eigenvalues (in absolute value). **f** CTMRG procedures updating the corner and edge tensors using the isometries.

infinite string lengths. Moreover, there is a small drop at the self-dual line in Fig. 4f, which slowly approaches 0 with increasing bond dimension; Fig. 4e.

Although surprising, the discontinuity in the flux condensed phase is possible because the FM string order parameter is a non-linear function of the ground state. The underlying reason for this abrupt change of the FM order parameter is that the parity of the dominant eigenvectors of the transfer matrices, whose overlap determines the FM order parameter, change at the discontinuity³⁰. In the Supplemental Materials³⁰, we show that for the Hamiltonian in Eq. (1) a similar singular behavior of the FM string order parameter can be found when calculating the FM order parameter using an iPEPS constructed via perturbing the infinite-field limit product states in the confined region⁶². These unexpected results indicate that in the flux condensation region, the FM string order parameter that creates charges at its end cannot be used as an order parameter anymore, and the FM string order parameter does not have a physical significance. We discuss the consequences of this behavior in the next section.

Discussion

We have evaluated the FM string order parameter in the infinitely long string limit using the iPEPS simulation and found that it exhibits universal scaling controlled by the underlying critical points of charge condensation transitions.

Our results indicate that the FM string order parameter can be discontinuous in the flux condensation region, which does not possess an emergent 1-form Wilson loop symmetry, see Fig. 4a and f. Hence, we argue that only in the presence of an emergent 1-form Wilson loop symmetry, the associated FM string order parameter can be a quantitatively well-behaved order parameter for topological phase transitions. Our argument can be formulated using the idea of quantum error correction^{63,64}. A quantum state $|\Psi\rangle$ having an emergent 1-form Wilson loop symmetry implies that we can apply a recovery map constructed from quantum error correction to $|\Psi\rangle$ to get an exact 1-form Wilson loop symmetric state $|\Psi_0\rangle$ within the same phase of $|\Psi\rangle$. Applying this recovery map to both the numerator and denominator of the FM order parameter, we have $\langle \Psi | \prod_{e \in L_{1/2}} Z_e | \Psi \rangle \sim e^{-\alpha |L_{1/2}|} \langle \Psi_0 | \prod_{e \in L_{1/2}} Z_e | \Psi_0 \rangle$ and $\langle \Psi | \prod_{e \in L_{1/2}} Z_e | \Psi \rangle \sim e^{-\alpha |L|}$ ⁶⁵, where α is a decay coefficient that depends on $|\Psi\rangle$ and the recovery map. The FM order parameter evaluated with $|\Psi\rangle$ using Eq. (3) then reduces to the string order parameter evaluated with $|\Psi_0\rangle$ using Eq. (2). As a consequence, the FM order parameter is a well-behaved order parameter in the presence of emergent 1-form Wilson loop symmetry. By contrast, if there is no emergent 1-form Wilson loop symmetry, it will not be guaranteed that a recovery map exists. In the confined regime, the magnetic 1-form 't Hooft loop symmetry is emergent, and one has to construct an FM order parameter of X operators along the dual lattice to detect the phase transition. Therefore, when detecting a topological phase transition using FM string order parameters, either with numerical simulations or experiments, knowledge about the underlying emergent 1-form symmetries is required.

Our work opens several questions and research directions. First, measuring the FM string order parameter in quantum simulation experiments can provide insights into topological phase transitions with charge condensation. Second, in ref. 65, we argue that 1-form symmetries can be detected with quantum error correction. It will be interesting to precisely analyze the boundaries of the three regions of different emergent 1-form symmetries in the trivial phase of the toric code model in Eq. (1), shown schematically in Fig. 1b, and investigate the nature of the transitions between presence and absence of the 1-form symmetries. Third, the FM string order parameter can be applied to different lattice gauge theories⁶⁶⁻⁶⁹. It is an interesting direction to define the FM string order parameters for Kitaev's quantum double models³ and Levin-Wen string-net models⁵ and apply them to study various topological phase transitions driven by anyon condensation^{50,51,70}. Moreover, since the Higgs phase can be interpreted as a phase protected simultaneously by both a 1-form symmetry and a global symmetry⁷¹, one could use the FM-type string order parameters to detect such kind of symmetry-protected topological order, especially when the protecting 1-form symmetry becomes an emergent symmetry⁷².

Methods

iPEPS optimization

In this section, we show the technical details of optimizing the ground states of the toric code model using iPEPS. We approximate a ground state using the iPEPS ansatz proposed in ref. 73. The iPEPS has a 2×2 unit cell, and it is parameterized by a rank-5 tensor A (B is obtained from A by a $\pi/2$ rotation) with the virtual bond dimension D and the physical dimension $d = 2$, as shown in Fig. 5a and b.

We impose the square lattice symmetry onto the tensor A such that the iPEPS tensor is invariant under two reflections R_v and R_h , see Fig. 5b. Because of the symmetry, the number of independent variational parameters is less than $2D^4$. We can parameterize such a symmetric tensor A using the following method. We first construct the $2D^4 \times 2D^4$ matrix representations of R_h and R_v applying on the tensor A , and a projector $P_R = (\mathbb{1} + R_h)(\mathbb{1} + R_v)/4$. A subspace spanned by the eigenvectors of P_R with an eigenvalue 1 is $\{|v_i\rangle | P_R |v_i\rangle = |v_i\rangle\}$. If $\langle v_i | v_j \rangle \neq \delta_{ij}$, we can orthonormalize them using the QR decomposition. Reshaping $|v_i\rangle$ to the tensors with the dimensions $D \times D \times D \times D \times 2$, we can parameterize the iPEPS tensor as $A = \sum_i \lambda_i |v_i\rangle$, where $\lambda = \{\lambda_i\}$ are variational parameters. If we also want to impose the virtual \mathbb{Z}_2 symmetry to the tensor A as shown in Fig. 5a, we need another projector $P_Z = (\mathbb{1}_D^{\otimes 4} \otimes \mathbb{1}_d + Z_D^{\otimes 4} \otimes \mathbb{1}_2)/2$, where Z_D is a $D \times D$ matrix representation of the non-trivial element in \mathbb{Z}_2 , i.e., $Z_D^2 = \mathbb{1}$; and we consider the projector $P = P_Z P_R$, where $[P_Z, P_R] = 0$. Using the orthonormal basis of the subspace spanned by the eigenvectors of P with eigenvalue 1, we can parameterize the tensor A using λ .

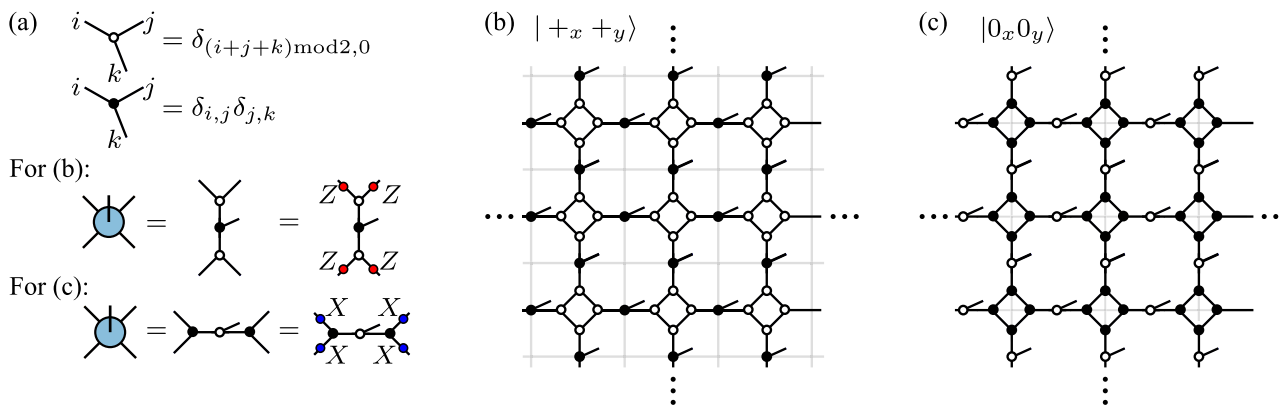


Fig. 6 | The exact iPEPS at the fixed point $h_x = h_z = 0$ of the toric code phase. **a** The two rank-3 three tensors are defined to construct the tensor A . The tensor A for $|+_{x+y}\rangle$ and $|0_x0_y\rangle$ has different virtual \mathbb{Z}_2 symmetry. iPEPS for **b** $|+_{x+y}\rangle$ and **c** $|0_x0_y\rangle$ on a torus. The gray lines indicate the primal lattice.

The iPEPS $|\Psi(\lambda)\rangle$ can be constructed from $A(\lambda)$. The energy expectation value $E = \langle \Psi(\lambda) | H_{TC}(h_z, h_x) | \Psi(\lambda) \rangle / \langle \Psi(\lambda) | \Psi(\lambda) \rangle$ can be evaluated by contracting iPEPS $|\Psi(\lambda)\rangle$. We contract (the squared norm of) the iPEPS using the corner transfer matrix renormalization group (CTMRG) algorithm. As shown in Fig. 5d, we approximate the environment of the double tensors (shown in Fig. 5c) in a 2×2 unit cell using corner (rectangles) and edge tensors (squares) with a bond dimension χ . Since we impose the square lattice symmetry to the tensor A , we can contract the iPEPS using the symmetric CTMRG⁷³. The bond dimensions of the corner and edge tensors grow to $D^2\chi$ after absorbing the double tensors, and we should truncate the bond dimension back to χ . Figure 5e shows that using hermitian eigenvalue decomposition we obtain the isometries (triangles), which can be used to truncate the bond dimensions, and we just use eigenvectors corresponding to the χ largest eigenvalues (in absolute value) to construct the isometry. With the isometries, we can update corner and edge tensors, as shown in Fig. 5f.

In order to optimize the iPEPS, one has to provide the energy gradient $\partial E / \partial \lambda$. The best way to calculate the energy gradient is using automatic differentiation (AD)²⁴, which calculates the gradient through a backward propagation along the computational graph based on the chain rule in calculus. One problem of applying AD to calculate $\partial E / \partial \lambda$ is that the gradient can be infinite when eigenvalues are degenerate. Although one can add a small perturbation to lift the degeneracy, numerical instability can still happen with a small probability. When we get an infinity gradient, we can detach the isometries from the computation graph and get an approximate gradient; a trade-off between the stability and the accuracy. A possibly better solution is to use the approaches shown in ref. 74.

Given the energy expectation value and its gradient, we use the BFGS (Broyden-Fletcher-Goldfarb-Shanno) algorithm to minimize the energy expectation value. When the optimization is converged, we have an iPEPS $|\Psi(\lambda)\rangle$ approximating a ground state of the toric code model. For this work, the iPEPS optimization was performed by PyTorch on the NVIDIA A100 80 GB GPU cards. We use the checkpoint function of PyTorch to reduce the huge memory cost of backward AD calculation. Moreover, when getting the isometries, we should use the hermitian eigenvalue decomposition rather than singular eigenvalue decomposition, because the former is about ten times faster than the latter on the GPU. It takes about two weeks (3 days) to calculate a single curve containing more than 100 data points with bond dimension $D = 5$ ($D = 4$) on a single A100 GPU card. Near critical points, CTMRG needs about 200 to 300 iterations to converge for a single energy evaluation.

iPEPS for topologically degenerate ground states

Here, we discuss two kinds of iPEPS representations of the toric code ground states. Understanding them is useful for initializing the iPEPS optimization and evaluating the FM string order parameter. When $h_x = h_z = 0$, the toric code Hamiltonian defined on a torus commutes with two Wilson loop

operators and two 't Hooft loop operators:

$$W_x^Z = \prod_{e \in L_x} Z_e, \quad W_y^Z = \prod_{e \in L_y} Z_e, \quad W_x^X = \prod_{e \in \hat{L}_x} X_e, \quad W_y^X = \prod_{e \in \hat{L}_y} X_e, \tag{5}$$

where L_x (L_y) is a non-contractible loop along x (y) direction on the primal lattice, and \hat{L}_x (\hat{L}_y) is a non-contractible loop along x (y) direction on the dual lattice. They satisfy

$$\begin{aligned} [W_x^Z, W_y^Z] &= [W_x^X, W_y^X] = [W_x^Z, W_x^X] = [W_y^Z, W_y^X] = 0, \\ \{W_x^Z, W_y^X\} &= \{W_x^X, W_y^Z\} = 0. \end{aligned} \tag{6}$$

The four ground states can be labeled by eigenvalues of a pair of two commuting loop operators, i.e., common eigenstates of W_x^Z and W_y^X :

$$|+_{x+y}\rangle, \quad |+_{x-y}\rangle, \quad |-_{x+y}\rangle, \quad |-_{x-y}\rangle, \tag{7}$$

or common eigenstates of W_x^Z and W_y^Z :

$$|0_x0_y\rangle, \quad |0_x1_y\rangle, \quad |1_x0_y\rangle, \quad |1_x1_y\rangle. \tag{8}$$

In particular, the common eigenstates of W_x^Z and W_x^X (alternatively one can use W_y^Z and W_y^X) are minimally entangled states⁴⁴:

$$|0_{x+}\rangle \equiv |1\rangle, \quad |1_{x+}\rangle \equiv |\mathbf{m}\rangle, \quad |0_{x-}\rangle \equiv |e\rangle, \quad |1_{x-}\rangle \equiv |f\rangle. \tag{9}$$

Let us focus on the ground states $|0_x0_y\rangle$ and $|+_{x+y}\rangle$, which can be exactly expressed in terms of the so-called "single-line" and "double-line" iPEPS with the toroidal boundary condition⁷⁵. They are included in the 2×2 unit cell iPEPS ansatz in Fig. 5a. As shown in Fig. 6a, by defining two of rank-3 tensors, we can obtain the A tensor for the iPEPS $|+_{x+y}\rangle$ shown in Fig. 6b or the iPEPS $|0_x0_y\rangle$ shown in Fig. 6c. Because the two kinds of nonequivalent of iPEPS representations of the fixed point toric code states are included in the 2×2 unit cell iPEPS ansatz, we expect that it performs better than other kinds of iPEPS ansatz for the toric code model, especially along the self-dual line.

When evaluating the FM string order parameter on a torus geometry for a non-contractible loop L , which as we have seen is convenient for our tensor network methods, the denominator in Eq. (3) depends on the choice of the topologically degenerate ground states in the toric code phase. This

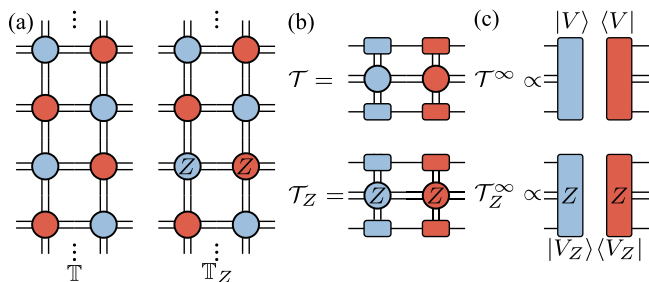


Fig. 7 | Evaluating the FM string order parameter using iPEPS. **a** Using the double tensors in Fig. 5c, two iPEPS transfer matrices are defined to evaluate the FM string order parameter. **b** Compressing the iPEPS transfer matrices using the edge tensors from the CTMRG. **c** The infinite power transfer matrices are given by their fixed points.

can be easily understood at the fixed point of the toric code phase. When using the ground state $|+_{x+y}\rangle$ to evaluate the FM string order parameter O_Z , we find that it is not well-defined because $|+_{x+y}\rangle$ spontaneously breaks the W_x^Z symmetry, i.e., $W_x^Z|+_{x+y}\rangle = |+_{x-y}\rangle$, such that the denominator $\langle +_{x+y} | W_x^Z | +_{x+y} \rangle = 0$. This problem can be circumvented by considering either the ground state $|0_{x,0_y}\rangle$ or the minimally entangled state of the trivial topological sector $|1\rangle$, such that the denominator of the FM string order parameter O_Z is 1. However, if we want to correctly evaluate FM string order parameters O_X and O_Z simultaneously, we have to consider the minimally entangled state $|1\rangle$. The FM string order parameters O_X and O_Z evaluated using the minimally entangled state in the trivial topological sector which mimics the one defined on a contractible loop.

Away from the fixed point of the toric code model, the exact Wilson and 't Hooft loop operators in Eq. (5) are not symmetries the Hamiltonian anymore. Since we mainly focus on the FM string order parameter O_Z , we just need to find the ground state $|0_{x,0_y}\rangle$, which is the simultaneous eigenstate of emergent non-contractible Wilson loop operators along x and y directions. Because the optimized iPEPS usually converge to $|0_{x,0_y}\rangle$ or $|+_{x+y}\rangle$, we can control which ground state it converges to by initializing the iPEPS tensor as $A + \epsilon R$, where A is given in Fig. 6a and R is a random tensor satisfying the required lattice symmetry, and ϵ is a small number. We emphasize that we do not imposing the virtual \mathbb{Z}_2 symmetry shown in Fig. 5b to the tensor during the optimization.

Evaluation of the FM string order parameter using iPEPS

With the optimized iPEPS tensor, we can evaluate the FM string order parameter efficiently in the limit of an infinitely long string using transfer matrices of iPEPS. To this end, we construct from the iPEPS of the ground state two transfer matrices; one is the usual transfer matrix \mathbb{T} and the other is \mathbb{T}_Z containing Z operators; see Fig. 7a for graphical notations. The numerator of the FM string order parameter consists of r transfer matrices \mathbb{T} followed by r transfer matrices \mathbb{T}_Z containing a Z string and the denominator consists of $2r$ transfer matrices \mathbb{T}_Z containing a Z loop:

$$O_Z = \lim_{r \rightarrow \infty} \left[\frac{\text{Tr}(\mathbb{T}^r \mathbb{T}_Z^r) / \text{Tr}(\mathbb{T}^{2r})}{\sqrt{\text{Tr}(\mathbb{T}_Z^{2r}) / \text{Tr}(\mathbb{T}^{2r})}} \right]^{1/2} \tag{10}$$

$$= \left[\lim_{r \rightarrow \infty} \frac{\text{Tr}(\mathbb{T}^r \mathbb{T}_Z^r) / \text{Tr}(\mathbb{T}^{2r})}{\sqrt{\text{Tr}(\mathbb{T}_Z^{2r}) / \text{Tr}(\mathbb{T}^{2r})}} \right]^{1/2}$$

$$= \lim_{r \rightarrow \infty} \frac{t_Z^r / t^r}{t_Z^{2r} / t^{2r}} |\langle V | V_Z \rangle| = |\langle V | V_Z \rangle|, \tag{11}$$

where we compress the transfer matrices \mathbb{T} and \mathbb{T}_Z to the transfer matrices \mathcal{T} and \mathcal{T}_Z with a dimension $D^2 \chi^2$ using the edge tensors from the CTMRG, see Fig. 7b, and t (t_Z), V (V_Z) are dominant eigenvalue and eigenvector of \mathcal{T} (\mathcal{T}_Z). Here, we assume that the dominant eigenvectors are non-degenerate and discuss the degenerate case later. In the limit of $r \rightarrow \infty$, the action of the transfer matrices is set by the dominating eigenvalue and eigenvector, $\mathcal{T}_Z^\infty = t_Z^\infty |V_Z\rangle\langle V_Z|$ and $\mathcal{T}^\infty = t^\infty |V\rangle\langle V|$, as shown in Fig. 7c, so Eq. (10) can be simplified to Eq. (11). Moreover, the perimeter law coefficient can be obtained from the dominant eigenvalues of the transfer matrices: $\alpha_Z = -\log(t_Z/t)$.

Next, we consider degenerate fixed points of \mathcal{T} and \mathcal{T}_Z . This could happen when a ground state in the toric code phase is chosen as the minimally entangled state. In the limit $r \rightarrow \infty$, \mathcal{T}^r (\mathcal{T}_Z^r) can be expressed as:

$$\mathcal{T}^\infty = \sum_{\alpha=1}^d t^\infty |V_\alpha\rangle\langle V_\alpha|, \quad \mathcal{T}_Z^\infty = \sum_{\alpha_Z=1}^{d_Z} t_Z^\infty |V_{Z,\alpha_Z}\rangle\langle V_{Z,\alpha_Z}|, \tag{12}$$

where d (d_Z) denotes the number of the dominant eigenvectors of \mathcal{T} and \mathcal{T}_Z , and α (α_Z) specifies the degenerate dominant vectors. Substituting Eq. (12) in Eq. (10), we can calculate the FM string order parameter even when the transfer matrix fixed points are degenerate:

$$O_Z = \left[\frac{1}{\sqrt{d d_Z}} \text{Tr} \left(\sum_{\alpha=1, \beta=1}^{d, d_Z} |V_{1,\alpha}\rangle\langle V_{1,\alpha} | V_{Z,\beta}\rangle\langle V_{Z,\beta} | \right) \right]^{1/2}. \tag{13}$$

Note Added

While finalizing the manuscript we became aware of related work on the stability of the FM order parameter⁷⁶.

Data availability

Data and data analysis are available upon reasonable request on Zenodo⁷⁷.

Code availability

Simulation code is available upon reasonable request on Zenodo⁷⁷.

Received: 12 July 2024; Accepted: 21 April 2025;

Published online: 09 May 2025

References

1. Tsui, D. C., Stormer, H. L. & Gossard, A. C. Two-dimensional magnetotransport in the extreme quantum limit. *Phys. Rev. Lett.* **48**, 1559 (1982).
2. Laughlin, R. B. Anomalous quantum hall effect: An incompressible quantum fluid with fractionally charged excitations. *Phys. Rev. Lett.* **50**, 1395 (1983).
3. Kitaev, A. Fault-tolerant quantum computation by anyons. *Ann. Phys.* **303**, 2 (2003).
4. Kitaev, A. Anyons in an exactly solved model and beyond. *Ann. Phys.* **321**, 2 (2006).
5. Levin, M. A. & Wen, X.-G. String-net condensation: A physical mechanism for topological phases. *Phys. Rev. B* **71**, 045110 (2005).
6. Wen, X.-G. A theory of 2+1D bosonic topological orders. *Natl. Sci. Rev.* **3**, 68 (2015).
7. Wen, X.-G. Colloquium: Zoo of quantum-topological phases of matter. *Rev. Mod. Phys.* **89**, 041004 (2017).

8. Satzinger, K. J. et al. Realizing topologically ordered states on a quantum processor. *Science* **374**, 1237 (2021).
9. Semeghini, G. et al. Probing topological spin liquids on a programmable quantum simulator. *Science* **374**, 1242 (2021).
10. Iqbal M. et al. Non-Abelian topological order and anyons on a trapped-ion processor. *Nature* **626**, 505 (2024).
11. Fredenhagen, K. & Marcu M. Charged states in \mathbb{Z}_2 gauge theories *Commun. Math. Phys.* **92**, 81–119 (1983).
12. Marcu, M. (uses of) an order parameter for lattice gauge theories with matter fields. *Lattice Gauge Theory: A Challenge in Large-Scale Computing* 267–278 (Springer, Boston, MA, 1986).
13. Fredenhagen, K. & Marcu, M. Confinement criterion for qcd with dynamical quarks. *Phys. Rev. Lett.* **56**, 223 (1986).
14. Fredenhagen, K. & Marcu, M. Dual interpretation of order parameters for lattice gauge theories with matter fields. *Nucl. Phys. B - Proc. Suppl.* **4**, 352 (1988).
15. Verresen, R., Lukin, M. D. & Vishwanath, A. Prediction of toric code topological order from rydberg blockade. *Phys. Rev. X* **11**, 031005 (2021).
16. Batista, C. D. & Nussinov, Z. Generalized elitzur's theorem and dimensional reductions. *Phys. Rev. B* **72**, 045137 (2005).
17. Hastings, M. B. & Wen, X.-G. Quasiadiabatic continuation of quantum states: The stability of topological ground-state degeneracy and emergent gauge invariance. *Phys. Rev. B* **72**, 045141 (2005).
18. Nussinov, Z. & Ortiz, G. A symmetry principle for topological quantum order. *Ann. Phys.* **324**, 977 (2009).
19. Gaiotto, D., Kapustin, A., Seiberg, N. & Willett, B. Generalized global symmetries. *J. High. Energy Phys.* **2015**, 1 (2015).
20. Wen, X.-G. Emergent anomalous higher symmetries from topological order and from dynamical electromagnetic field in condensed matter systems. *Phys. Rev. B* **99**, 205139 (2019).
21. McGreevy, J. Generalized symmetries in condensed matter. *Annu. Rev. Condens. Matter Phys.* **14**, 57 (2023).
22. Vanderstraeten, L., Haegeman, J., Corboz, P. & Verstraete, F. Gradient methods for variational optimization of projected entangled-pair states. *Phys. Rev. B* **94**, 155123 (2016).
23. Corboz, P. Variational optimization with infinite projected entangled-pair states. *Phys. Rev. B* **94**, 035133 (2016).
24. Liao, H.-J., Liu, J.-G., Wang, L. & Xiang, T. Differentiable programming tensor networks. *Phys. Rev. X* **9**, 031041 (2019).
25. Schuler, M., Whitsitt, S., Henry, L.-P., Sachdev, S. & Läuchli, A. M. Universal signatures of quantum critical points from finite-size torus spectra: A window into the operator content of higher-dimensional conformal field theories. *Phys. Rev. Lett.* **117**, 210401 (2016).
26. Somoza, A. M., Serna, P. & Nahum, A. Self-dual criticality in three-dimensional \mathbb{Z}_2 gauge theory with matter. *Phys. Rev. X* **11**, 041008 (2021).
27. Bonati, C., Pelissetto, A. & Vicari, E. Multicritical point of the three-dimensional \mathbb{Z}_2 gauge higgs model. *Phys. Rev. B* **105**, 165138 (2022).
28. Oppenheim, L., Koch-Janusz, M., Gazit, S. & Ringel, Z. Machine learning the operator content of the critical self-dual ising-higgs gauge model. *Phys. Rev. Research* **6**, 043322 (2024).
29. Bonati, C., Pelissetto, A. & Vicari, E. Comment on “machine learning the operator content of the critical self-dual ising-higgs gauge model”, arxiv:2311.17994v1 <https://arxiv.org/abs/2401.10563> (2024).
30. See Supplemental Material for the benchmark iPEPS results using the QMC results, discontinuity of the FM string order parameter, the dual FM string order parameter, equivalence between the FM string order parameters defined using contractible and non-contractible loops, and analysis of the FM order parameters for the deformed wavefunction.
31. Linsell, S. M., Bohrdt, A., Homeier, L., Pollet, L. & Grusdt, F. Percolation as a confinement order parameter in \mathbb{Z}_2 lattice gauge theories. *Phys. Rev. B* **110**, L241101 (2024).
32. Wu, F., Deng, Y. & Prokof'ev, N. Phase diagram of the toric code model in a parallel magnetic field. *Phys. Rev. B* **85**, 195104 (2012).
33. Vidal, J., Dusuel, S. & Schmidt, K. P. Low-energy effective theory of the toric code model in a parallel magnetic field. *Phys. Rev. B* **79**, 033109 (2009).
34. Dusuel, S., Kamfor, M., Orús, R., Schmidt, K. P. & Vidal, J. Robustness of a perturbed topological phase. *Phys. Rev. Lett.* **106**, 107203 (2011).
35. Pace, S. D. & Wen, X.-G. Exact emergent higher-form symmetries in bosonic lattice models. *Phys. Rev. B* **108**, 195147 (2023).
36. The broken emergent 1-form symmetry defined on a non-contractible loop can be restored using minimally entangled states. Also, notice that the emergent Wilson loop symmetry defined on a contractible loop is unbroken for any ground state.
37. Bricmont, J. & Frölich, J. An order parameter distinguishing between different phases of lattice gauge theories with matter fields. *Phys. Lett. B* **122**, 73 (1983).
38. Wegner, F. J. Duality in generalized ising models and phase transitions without local order parameters. *J. Math. Phys.* **12**, 2259 (1971).
39. Trebst, S., Werner, P., Troyer, M., Shtengel, K. & Nayak, C. Breakdown of a topological phase: Quantum phase transition in a loop gas model with tension. *Phys. Rev. Lett.* **98**, 070602 (2007).
40. Blöte, H. W. J. & Deng, Y. Cluster monte carlo simulation of the transverse ising model. *Phys. Rev. E* **66**, 066110 (2002).
41. Kos, F., Poland, D., Simmons-Duffin, D. & Vichi, A. Precision islands in the ising and o (n) models. *J. High. Energy Phys.* **2016**, 1 (2016).
42. Cian, Z.-P., Hafezi, M. & Barkeshli, M. Extracting wilson loop operators and fractional statistics from a single bulk ground state <https://arxiv.org/abs/2209.14302> (2022).
43. Cong Iris, et. al. Enhancing detection of topological order by local error correction. *Nat. Commun.* **15**, 1527 (2024).
44. Zhang, Y., Grover, T., Turner, A., Oshikawa, M. & Vishwanath, A. Quasiparticle statistics and braiding from ground-state entanglement. *Phys. Rev. B* **85**, 235151 (2012).
45. Corboz, P., Czarnik, P., Kapteijns, G. & Tagliacozzo, L. Finite correlation length scaling with infinite projected entangled-pair states. *Phys. Rev. X* **8**, 031031 (2018).
46. Rader, M. & Läuchli, A. M. Finite correlation length scaling in lorentz-invariant gapless ipeps wave functions. *Phys. Rev. X* **8**, 031030 (2018).
47. Vanhecke, B., Hasik, J., Verstraete, F. & Vanderstraeten, L. Scaling hypothesis for projected entangled-pair states. *Phys. Rev. Lett.* **129**, 200601 (2022).
48. Iqbal, M., Duivenvoorden, K. & Schuch, N. Study of anyon condensation and topological phase transitions from a z_4 topological phase using the projected entangled pair states approach. *Phys. Rev. B* **97**, 195124 (2018).
49. Duivenvoorden, K., Iqbal, M., Haegeman, J., Verstraete, F. & Schuch, N. Entanglement phases as holographic duals of anyon condensates. *Phys. Rev. B* **95**, 235119 (2017).
50. Xu, W.-T. & Schuch, N. Characterization of topological phase transitions from a non-abelian topological state and its galois conjugate through condensation and confinement order parameters. *Phys. Rev. B* **104**, 155119 (2021).
51. Xu, W.-T., Garre-Rubio, J. & Schuch, N. Complete characterization of non-abelian topological phase transitions and detection of anyon splitting with projected entangled pair states. *Phys. Rev. B* **106**, 205139 (2022).
52. Iqbal, M. & Schuch, N. Entanglement order parameters and critical behavior for topological phase transitions and beyond. *Phys. Rev. X* **11**, 041014 (2021).
53. Schuch, N., Cirac, I. & Pérez-García, D. Peps as ground states: Degeneracy and topology. *Ann. Phys.* **325**, 2153 (2010).
54. Bultinck, N. et al. Anyons and matrix product operator algebras. *Ann. Phys.* **378**, 183 (2017).
55. Şahinoğlu, M. B. et al. Characterizing topological order with matrix product operators, in *Annales Henri Poincaré*, Vol. 22 (Springer, 2021) pp. 563–592.

56. Claudio Castelnovo, M. T. Simon Trebst Topological order and quantum criticality, in *Understanding Quantum Phase Transitions* (CRC Press, 2010) p. 119–142.
57. Isakov, S. V., Fendley, P., Ludwig, A. W. W., Trebst, S. & Troyer, M. Dynamics at and near conformal quantum critical points. *Phys. Rev. B* **83**, 125114 (2011).
58. Haegeman, J., Zauner, V., Schuch, N. & Verstraete, F. Shadows of anyons and the entanglement structure of topological phases. *Nat. Commun.* **6**, 8284 (2015).
59. Haegeman, J., Van Acoleyen, K., Schuch, N., Cirac, J. I. & Verstraete, F. Gauging quantum states: From global to local symmetries in many-body systems. *Phys. Rev. X* **5**, 011024 (2015).
60. Zhu, G.-Y. & Zhang, G.-M. Gapless coulomb state emerging from a self-dual topological tensor-network state. *Phys. Rev. Lett.* **122**, 176401 (2019).
61. Henriksson, J. The critical $o(n)$ cft: Methods and conformal data. *Phys. Rep.* **1002**, 1 (2023). the critical $O(N)$ CFT: Methods and conformal data.
62. Vanderstraeten, L. et al. Bridging perturbative expansions with tensor networks. *Phys. Rev. Lett.* **119**, 070401 (2017).
63. Lavasani, A. & Vijay, S. The stability of gapped quantum matter and error-correction with adiabatic noise. <http://arxiv.org/abs/2402.14906> (2024).
64. Serna, P., Somoza, A. M. & Nahum, A. Worksheet patching 1-form symmetries and Landau * phase transitions. *Phys. Rev. B* **110**, 115102 (2024).
65. Liu, Y.-J., Xu, W.-T., Pollmann, F. & Knap, M., Detecting emergent 1-form symmetries with quantum error correction. <https://arxiv.org/abs/2502.17572> (2025).
66. Gregor, K., Huse, D. A., Moessner, R. & Sondhi, S. L. Diagnosing deconfinement and topological order. *N. J. Phys.* **13**, 025009 (2011).
67. Cobanera, E., Ortiz, G. & Nussinov, Z. Holographic symmetries and generalized order parameters for topological matter. *Phys. Rev. B* **87**, 041105 (2013).
68. Liu, K. et al. Classification of nematic order in $2 + 1$ dimensions: Dislocation melting and $o(2)/Z_N$ lattice gauge theory. *Phys. Rev. B* **91**, 075103 (2015).
69. Beekman, A. et al. Dual gauge field theory of quantum liquid crystals in two dimensions. *Phys. Rep.* **683**, 1 (2017).
70. Xu, W.-T., Zhang, Q. & Zhang, G.-M. Tensor network approach to phase transitions of a non-abelian topological phase. *Phys. Rev. Lett.* **124**, 130603 (2020).
71. Verresen, R., Borla, U., Vishwanath, A., Moroz, S. & Thorngren, R. Higgs condensates are symmetry-protected topological phases: I. discrete symmetries <http://arxiv.org/abs/2211.01376> (2022).
72. Xu, W.-T., Rakovszky T., Knap M. & Pollmann F. Entanglement Properties of Gauge Theories from Higher-Form Symmetries. *Phys. Rev. X* **15**, 011001 (2025).
73. Crone, S. P. G. & Corboz, P. Detecting a Z_2 topologically ordered phase from unbiased infinite projected entangled-pair state simulations. *Phys. Rev. B* **101**, 115143 (2020).
74. Francuz, A., Schuch, N. & Vanhecke, B. Stable and efficient differentiation of tensor network algorithms. *Phys. Rev. Research* **7**, 013237 (2025).
75. Gu, Z.-C., Levin, M. & Wen, X.-G. Tensor-entanglement renormalization group approach as a unified method for symmetry breaking and topological phase transitions. *Phys. Rev. B* **78**, 205116 (2008).
76. Verresen, R., Vishwanath, A. & Schuch, N. In preparation (2024).
77. Xu, W.-T., Pollmann, F. & Knap, M. Critical behavior of the Fredenhagen-Marcu order parameter for topological phase transitions, <https://doi.org/10.5281/zenodo.10494400> (2024).
78. Francesco, P., Mathieu, P. & Sénéchal, D. *Conformal field theory* (Springer Science & Business Media, 2012).
79. Chester, S. M. et al. Carving out open space and precise $o(2)$ model critical exponents. *J. High. Energy Phys.* **2020**, 1 (2020).
80. Nienhuis, B. Exact critical point and critical exponents of $O(n)$ models in two dimensions. *Phys. Rev. Lett.* **49**, 1062 (1982).
81. Di Francesco, P., Saleur, H. & Zuber, J.-B. Relations between the coulomb gas picture and conformal invariance of two-dimensional critical models. *J. Stat. Phys.* **49**, 57 (1987).

Acknowledgements

We thank Fengcheng Wu and Youjin Deng for providing their original QMC data used in ref. 32, and Tibor Rakovszky, Yu-Jie Liu and Rui-Zhen Huang for many helpful comments. We acknowledge support from the Deutsche Forschungsgemeinschaft (DFG, German Research Foundation) under Germany's Excellence Strategy—EXC—2111—390814868, TRR 360 - 492547816 and DFG grants No. KN1254/1-2, KN1254/2-1, the European Research Council (ERC) under the European Union's Horizon 2020 research and innovation programme (grant agreement No. 851161 and No. 771537), as well as the Munich Quantum Valley, which is supported by the Bavarian state government with funds from the Hightech Agenda Bayern Plus.

Author contributions

W.-T. X. developed the codes and performed the numerical simulations. All authors contributed to the discussion of the results and the writing of the manuscript.

Funding

Open Access funding enabled and organized by Projekt DEAL.

Competing interests

The authors declare no competing interests.

Additional information

Supplementary information The online version contains supplementary material available at <https://doi.org/10.1038/s41534-025-01030-z>.

Correspondence and requests for materials should be addressed to Wen-Tao Xu.

Reprints and permissions information is available at <http://www.nature.com/reprints>

Publisher's note Springer Nature remains neutral with regard to jurisdictional claims in published maps and institutional affiliations.

Open Access This article is licensed under a Creative Commons Attribution 4.0 International License, which permits use, sharing, adaptation, distribution and reproduction in any medium or format, as long as you give appropriate credit to the original author(s) and the source, provide a link to the Creative Commons licence, and indicate if changes were made. The images or other third party material in this article are included in the article's Creative Commons licence, unless indicated otherwise in a credit line to the material. If material is not included in the article's Creative Commons licence and your intended use is not permitted by statutory regulation or exceeds the permitted use, you will need to obtain permission directly from the copyright holder. To view a copy of this licence, visit <http://creativecommons.org/licenses/by/4.0/>.

© The Author(s) 2025